

Double-charm and hidden-charm hexaquark states under the complex scaling method

Jian-Bo Cheng^{1,*}, Du-xin Zheng^{2,†}, Zi-Yang Lin^{1,‡} and Shi-Lin Zhu^{1,§}

¹*School of Physics and Center of High Energy Physics, Peking University 100871, China*

²*Shandong Institute of Advanced Technology, Jinan 250100, China*

(Dated: November 10, 2022)

We investigate the double-charm and hidden-charm hexaquarks as molecules in the framework of the one-boson-exchange potential model. The multichannel coupling and $S - D$ wave mixing are taken into account carefully. We adopt the complex scaling method to investigate the possible quasibound states, whose widths are from the three-body decay channel $\Lambda_c \Lambda_c \pi$ or $\Lambda_c \bar{\Lambda}_c \pi$. For the double-charm system of $I(J^P) = 1(1^+)$, we obtain a quasibound state, whose width is 0.50 MeV if the binding energy is -14.27 MeV. And the S -wave $\Lambda_c \Sigma_c$ and $\Lambda_c \Sigma_c^*$ components give the dominant contributions. For the $1(0^+)$ double-charm hexaquark system, we do not find any pole. We find more poles in the hidden-charm hexaquark system. We obtain one pole as a quasibound state in the $I^G(J^{PC}) = 1^+(0^{--})$ system, which only has one channel $(\Lambda_c \bar{\Sigma}_c + \Sigma_c \bar{\Lambda}_c)/\sqrt{2}$. Its width is 1.72 MeV with a binding energy of -5.37 MeV. But, we do not find any pole for the scalar $1^-(0^{++})$ system. For the vector $1^-(1^{++})$ system, we find a quasibound state. Its energies, widths and constituents are very similar to those of the $1(1^+)$ double-charm case. In the vector $1^+(1^{--})$ system, we get two poles—a quasibound state and a resonance. The quasibound state has a width of 0.6 MeV with a binding energy of -15.37 MeV. For the resonance, its width is 2.72 MeV with an energy of 63.55 MeV relative to the $\Lambda_c \bar{\Sigma}_c$ threshold. And its partial width from the two-body decay channel $(\Lambda_c \bar{\Sigma}_c - \Sigma_c \bar{\Lambda}_c)/\sqrt{2}$ is apparently larger than the partial width from the three-body decay channel $\Lambda_c \bar{\Lambda}_c \pi$. Especially, the $1^+(0^{--})$ and $1^-(1^{++})$ hidden-charm hexaquark molecular states are very interesting. These isovector mesons have exotic J^{PC} quantum numbers which are not accessible to the conventional $q\bar{q}$ mesons.

I. INTRODUCTION

In the study of the hadronic molecular states, the dibaryon always plays an important role. The well-known deuteron is the only experimentally confirmed baryon-baryon bound state without charm quarks. Moreover, the WASA-at-COSY Collaboration repeatedly observed the dibaryon resonance $d^*(2380)$ [1–5]. It is natural to extend the investigation from the deuteron to the strange dibaryon. Jaffe suggested the famous H-dibaryon composed of the $\Lambda\Lambda$ pair [6], which was also studied in a series of works [6–20]. Besides, the dibaryon with one heavy quark ($qqqqqQ$) was also investigated in Refs. [21–23].

In 2017, the LHCb Collaboration discovered a double-charm baryon in the $\Lambda_c^+ K^- \pi^+ \pi^-$ mass spectrum— Ξ_{cc}^{++} [24], which is also the first observed double-heavy hadron. This discovery encouraged the research on the double-heavy hadrons, especially the double-charm tetraquarks [25–33]. After four years, the LHCb Collaboration reported the observation of the first double-heavy exotic hadron— T_{cc}^+ [34, 35]. After the rapid succession of the double-charm hadron discovery, it is necessary to implement a further investigation. We will focus on the double-charm deuteron-like hexaquarks in this work.

In the molecule picture, the double-charm dibaryon could be easier to form a bound state due to the larger reduced mass. And in fact, the double-heavy hexaquark ($qqqqqQ$) systems have been discussed in various approaches [36–54], including the chiral constituent quark model [36, 37], the quark delocalization color screening model [38, 39], the chromomagnetic model [40], the QCD sum rules [41], the chiral effective field theory (EFT) [42, 43], and the one-boson-exchange (OBE) model [44–50]. For the $\Lambda_c \Sigma_c$ molecule system, the authors of Ref. [46] found a bound state with the number $I(J^P) = 1(1^+)$. However, it was not confirmed in Ref. [39]. The hidden-heavy hexaquark ($qqQ\bar{q}\bar{q}\bar{Q}$) may have similar behaviors, and the relevant investigations can be found in Refs. [52, 55–60].

In this work, we investigate the double-charm dibaryon and hidden-charm baryonium systems containing the $\Lambda_c \Sigma_c^{(*)}$ and $\Lambda_c \bar{\Sigma}_c^{(*)}$ channels in the molecule picture. As pointed out in our previous work [61], the cross diagram $DD^* \leftrightarrow D^*D$ of the one-pion-exchange will provide a complex potential, which is from the three-body decay effect. This behavior

*Electronic address: jcheng@pku.edu.cn

†Electronic address: duxin.zheng@iat.cn

‡Electronic address: lzy_15@pku.edu.cn

§Electronic address: zhushl@pku.edu.cn

could also occur in the process $\Lambda_c \Sigma_c^{(*)} \leftrightarrow \Sigma_c^{(*)} \Lambda_c$. To study the possible three-body effect, we will retain the imaginary contribution from the OPE potential.

We use the OBE model to deal with the molecule state system. In order to explore the existence of the resonance, we will adopt the complex scaling method (CSM) [62, 63], which is a powerful method that can handle the bound state and resonance in a consistent way. Besides, the $S-D$ wave mixing and coupled-channel effect will be considered in this work. For both the double-charm and hidden-charm hexaquarks, the dominant contributions of the widths arise from the open-charm decay processes. The possible hidden-charm decay contributions for the hidden-charm hexaquark systems are negligible.

This paper is organized as follows. In Sec. II, we will introduce our framework explicitly. In Sec. III, we present the effective Lagrangians and potentials. In Sec. IV, we solve the complex scaled Schrödinger equation and give the results of the double-charm dibaryon and hidden-charm baryonium. The last section V is a brief summary.

II. FRAMEWORK

In the previous work [61], we studied the double-charm tetraquark with the CSM method. The DD^* system is found to be special since the 0th component of the transferred momentum of the exchanged pion is larger than the pion mass. This feature will provide the OPE potential with an imaginary part. If one could get a pole in this system, one may get an energy with an imaginary part which is explained as its half width. Therefore, we will pay more attention to the systems containing this type of interaction. One could see similar interactions in several systems, such as $\Lambda_c \Sigma_c \leftrightarrow \Sigma_c \Lambda_c$, $\Lambda_c \bar{\Sigma}_c \leftrightarrow \Sigma_c \bar{\Lambda}_c$, $\Lambda_c D^* \leftrightarrow \Sigma_c D$ and $\Lambda_c \bar{D}^* \leftrightarrow \Sigma_c \bar{D}$. In this work, we consider the former two cases: the double-charm and hidden-charm hexaquark molecule system.

To find the possible bound and resonant states, we take into account coupled-channel effect. The explicit systems and channels can be seen in Table I. However, we do not consider the isoscalar system with channels $\Lambda_c \Lambda_c$, $\Sigma_c \Sigma_c$ and $\Sigma_c^* \Sigma_c^*$ (or $\Lambda_c \bar{\Lambda}_c$, $\Sigma_c \bar{\Sigma}_c$ and $\Sigma_c^* \bar{\Sigma}_c^*$) in this work. Unlike the other two isovector systems, this system does not have the special cross diagram and could not contribute an imaginary part to the OPE potential. We will study these systems in the subsequent work. For the isovector cases, we will not take into account channels $\Sigma_c \Sigma_c^*$ and $\Sigma_c^* \Sigma_c^*$ (or $\Sigma_c \bar{\Sigma}_c^*$ and $\Sigma_c^* \bar{\Sigma}_c^*$) due to the same reason. In this work, we only consider the channels with 1S_0 ($J=0$), 3S_1 ($J=1$) and 3D_1 ($J=1$).

The masses of the charmed baryon and exchanged light mesons are shown in Table II. We take the isospin mean masses to deal with the isospin conservation process.

	$I^G(J^{PC})$	1	2	3	4	5	6
cc	$0(0^+)$	$\Lambda_c \Lambda_c(^1S_0)$	$\Sigma_c \Sigma_c(^1S_0)$	$\Sigma_c^* \Sigma_c^*(^1S_0)$			
	$1(0^+)$	$\Lambda_c \Sigma_c(^1S_0)$					
	$1(1^+)$	$\Lambda_c \Sigma_c(^3S_1)$	$\Lambda_c \Sigma_c(^3D_1)$	$\Lambda_c \Sigma_c^*(^3S_1)$	$\Lambda_c \Sigma_c^*(^3D_1)$	$\Sigma_c \Sigma_c(^3S_1)$	$\Sigma_c \Sigma_c(^3D_1)$
$c\bar{c}$	$0^+(0^{-+})$	$\Lambda_c \bar{\Lambda}_c(^1S_0)$	$\Sigma_c \bar{\Sigma}_c(^1S_0)$	$\Sigma_c^* \bar{\Sigma}_c^*(^1S_0)$			
	$1^+(0^{--})$	$\{\Lambda_c \bar{\Sigma}_c\}(^1S_0)$					
	$1^-(0^{-+})$	$[\Lambda_c \bar{\Sigma}_c](^1S_0)$	$\Sigma_c \bar{\Sigma}_c(^1S_0)$				
	$1^+(1^{--})$	$[\Lambda_c \bar{\Sigma}_c](^3S_1)$	$[\Lambda_c \bar{\Sigma}_c](^3D_1)$	$\{\Lambda_c \bar{\Sigma}_c^*\}(^3S_1)$	$\{\Lambda_c \bar{\Sigma}_c^*\}(^3D_1)$	$\Sigma_c \bar{\Sigma}_c(^3S_1)$	$\Sigma_c \bar{\Sigma}_c(^3D_1)$
	$1^-(1^{-+})$	$\{\Lambda_c \bar{\Sigma}_c\}(^3S_1)$	$\{\Lambda_c \bar{\Sigma}_c\}(^3D_1)$	$[\Lambda_c \bar{\Sigma}_c^*](^3S_1)$	$[\Lambda_c \bar{\Sigma}_c^*](^3D_1)$		

TABLE I: The channels of the double- and hidden-charm hexaquark systems. We adopt the following shorthand notations for simplicity, $[\Lambda_c \bar{\Sigma}_c^{(*)}] = \frac{1}{\sqrt{2}}(\Lambda_c \bar{\Sigma}_c^{(*)} - \Sigma_c^{(*)} \bar{\Lambda}_c)$ and $\{\Lambda_c \bar{\Sigma}_c^{(*)}\} = \frac{1}{\sqrt{2}}(\Lambda_c \bar{\Sigma}_c^{(*)} + \Sigma_c^{(*)} \bar{\Lambda}_c)$.

A. A brief discussion on the CSM

We first briefly introduce the CSM before investigating the analyticity of the OPE potentials. Aguilar, Balslev, and Combes proposed this method in the 1970s [62, 63], and the corresponding conclusion is known as the ABC theorem.

Mesons	Mass(MeV)	Mesons	Mass(MeV)
Λ_c^+	2286.46	σ	600
Σ_c^{++}	2453.97	π^\pm	139.57
Σ_c^+	2452.65	π^0	134.98
Σ_c^0	2453.75	η	547.86
Σ_c^{*++}	2518.41	ρ	775.26
Σ_c^{*+}	2517.4	ω	782.66
Σ_c^{*0}	2518.48		

TABLE II: The masses of the charmed baryons and exchanged light mesons in the OBE potential, which are taken from the PDG [64].

In this powerful method, the resonances can be solved in the same way as the bound states. The transformation of the radial coordinate r and its conjugate momentum k in the CSM is defined by:

$$U(\theta)r = re^{i\theta}, \quad U(\theta)k = ke^{-i\theta}. \quad (1)$$

Then the radial Schrödinger equation is transformed as

$$\left\{ \frac{1}{2m} \left[-\frac{d^2}{dr^2} + \frac{l(l+1)}{r^2} \right] e^{-2i\theta} + V(re^{i\theta}) \right\} \psi_l^\theta(r) = E(\theta) \psi_l^\theta(r). \quad (2)$$

After the complex scaling operation, the resonance pole would cross the branch cut into the first Riemann sheet if the rotation angle θ is large enough, as shown in Fig. 1. In this way, the wave functions of the resonances become square-integrable, just like the normalizable bound states. The details can be seen in Ref. [65, 66].

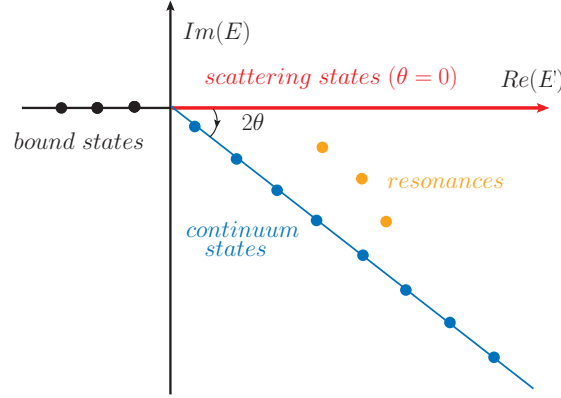


FIG. 1: The eigenvalue distribution of the complex scaled Schrödinger equation for two-body systems.

In the previous work [61], we adopted the Gaussian expansion method (GEM) [67] to solve the tetraquark system and our results agreed with the experimental data very well. However, when dealing with resonances, the GEM may not be applicable to some extreme situations. For example, if there is a pole located on the second Riemann sheet corresponding to one of the channels, we need to make a complex scaling to move this pole to the first Riemann sheet. And when this pole is too close to or below the threshold, the rotation angle $\theta \gtrsim \pi/4$, which is out of the limit of the Gaussian basis. So we adopt another function as the basis sets—the Laguerre functions of the form

$$\phi_{nl}(\lambda r) = \sqrt{\frac{n!}{(2l+2+n)!}} (\lambda r)^{l+1} e^{-\lambda r/2} L_n^{2l+2}(\lambda r), \quad (3)$$

where the λ is an adjustable parameter for the different size state. The radial wave function can be expanded as

$$\psi_l^\theta(r) = \sum_n^N c_n(\theta) \phi_{nl}(\lambda r), \quad (4)$$

where the $c_n(\theta)$ is the rotation angle θ -dependent coefficient. These basis sets have some good characteristics: 1) We could get all the resonances located on the second Riemann sheets since the angle region becomes $0 < \theta < \pi/2$. 2) The basis functions are orthonormal. 3) One could evaluate all the Hamiltonian matrix elements with simple analytical formulas in the OBE potential case. 4) These basis sets could allow the wave function to have the oscillating behavior of trigonometric function in a infinite range so that one could get the partial width of the corresponding resonance with the Golden rule [68, 69]. One could find the concrete application in Ref. [70].

B. Analyticity of the OPE potentials for the $\Lambda_c \Sigma_c^{(*)}$ system

When considering the process $\Lambda_c \Sigma_c \rightarrow \Sigma_c \Lambda_c$, one can get potentials as follows

$$V_\pi \propto \frac{1}{2f_\pi^2} \frac{(\boldsymbol{\sigma} \cdot \mathbf{q})(\boldsymbol{\sigma} \cdot \mathbf{q})}{q^2 - m_\pi^2}, \quad (5)$$

where the $\boldsymbol{\sigma}$ is the Pauli matrix. The q is the transferred momentum of the pion, and the q_0 is its 0th component. The denominator above gives $q^2 - m_\pi^2 = -(\mathbf{q}^2 - m_{eff}^2)$, where the shorthand $m_{eff} = \sqrt{q_0^2 - m_\pi^2}$ and the $q_0 \approx m_{\Sigma_c} - m_{\Lambda_c} > m_\pi$. Obviously, the poles are located on the real transferred momentum axis. When making a Fourier transformation, we adopt Feynman prescription to make the contour integral, and the OPE potential is proportional to $1/(\mathbf{p}^2 - m_{eff}^2 - i\epsilon)$. It is obvious that the complex scaling operation will not change the analyticity of the OPE potential. Compared with the DD^* system, we have an additional channel $\Lambda_c \Sigma_c^*$ that could provide a similar potential. The processes $\Lambda_c \Sigma_c^* \rightarrow \Sigma_c^* \Lambda_c$ and $\Lambda_c \Sigma_c \rightarrow \Sigma_c^* \Lambda_c$ could contribute an imaginary part too. To discuss this type of process, we make a careful discussion on the q_0 herein. Since $m_{\Sigma_c} - m_{\Lambda_c}$ and m_π are comparable, the effective mass $m_{eff} \approx \sqrt{2m_\pi(m_{\Sigma_c} - m_{\Lambda_c} - m_\pi)}$ is small. Therefore, the small bound energy could also affect the m_{eff} . To deal with the q_0 in the $\Lambda_c \Sigma_c^{(*)} \rightarrow \Sigma_c^{(*)} \Lambda_c$ process, we denote the total energy as E and assume the Λ_c to be on shell. Then the $q_0 = E - \sqrt{m_{\Lambda_c}^2 + \mathbf{p}^2} - \sqrt{m_{\Lambda_c}^2 + \mathbf{p}'^2}$, as illustrated in Fig. 2(a).

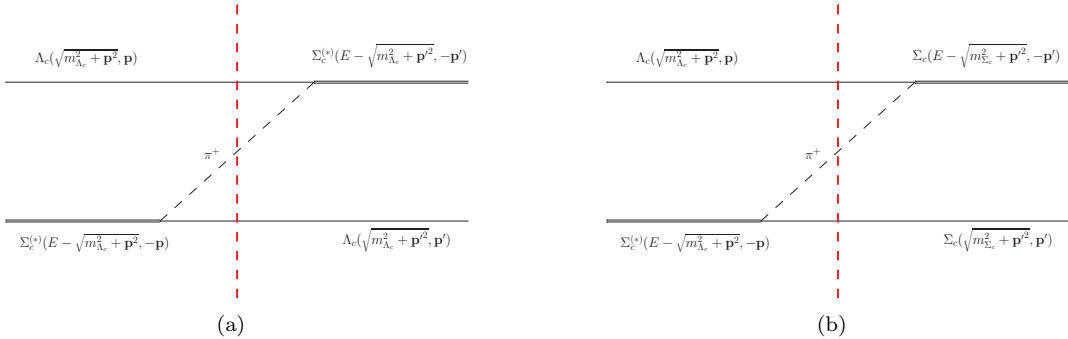


FIG. 2: Three-body intermediate state diagram in the processes (a) $\Lambda_c \Sigma_c^{(*)} \rightarrow \Sigma_c^{(*)} \Lambda_c$ and (b) $\Lambda_c \Sigma_c^{(*)} \rightarrow \Sigma_c \Sigma_c$. We assume the total energy is E , and the baryons cut by the red dashed line are on shell.

We will neglect the kinetic energy terms $\mathbf{p}^2/2m_{\Lambda_c}$ and $\mathbf{p}'^2/2m_{\Lambda_c}$ of the charmed baryons due to the heavy quark approximation. Then we make an energy shift $E \rightarrow E + 2m_{\Lambda_c}$, and the q_0 gives $q_0 = E + m_{\Sigma_c} - m_{\Lambda_c}$. For the process containing the $\Sigma_c \Sigma_c$ channel, we take $q_0 = 0$ in the diagonal process $\Sigma_c \Sigma_c \rightarrow \Sigma_c \Sigma_c$ and $q_0 = E$ in the non-diagonal process $\Lambda_c \Sigma_c^{(*)} \rightarrow \Sigma_c \Sigma_c$. We illustrate the latter one in Fig. 2(b). In this work, the latter one could also provide an imaginary part when the energy is around the threshold of the $\Sigma_c \Sigma_c$. In fact, we also use these assumptions in the process with other propagators. We list q_0 values for different cases in Table III. To distinguish the special q_0 in the cross diagrams $\Lambda_c \Sigma_c^{(*)} \rightarrow \Sigma_c^{(*)} \Lambda_c$ from the q_0 in the direct diagrams $\Lambda_c \Sigma_c^{(*)} \rightarrow \Lambda_c \Sigma_c^{(*)}$, we use the shorthand " q_0^C " for the former cases when we give concrete expressions of the potentials.

Process	$\Lambda_c \Sigma_c^{(*)} \rightarrow \Sigma_c^{(*)} \Lambda_c$	$\Lambda_c \Sigma_c^{(*)} \rightarrow \Sigma_c \Sigma_c$
q_0	$E + m_{\Sigma_c} - m_{\Lambda_c}$	E
Process	$\Lambda_c \bar{\Sigma}_c^{(*)} \rightarrow \Sigma_c^{(*)} \bar{\Lambda}_c$	$\Lambda_c \bar{\Sigma}_c^{(*)} \rightarrow \Sigma_c \bar{\Sigma}_c$
q_0	$E + m_{\Sigma_c} - m_{\Lambda_c}$	E

TABLE III: The q_0 is the 0th component of the transferred momentum. The E is the total energy relative to the threshold of the $\Lambda_c \Sigma_c$. The $q_0 = E + m_{\Sigma_c} - m_{\Lambda_c}$ is from the cross diagram $\Lambda_c \Sigma_c^{(*)} \rightarrow \Sigma_c^{(*)} \Lambda_c$. And the q_0 from the direct diagram $\Lambda_c \Sigma_c^{(*)} \rightarrow \Lambda_c \Sigma_c^{(*)}$ is equal to 0. The cases not listed all give $q_0 = 0$.

III. LAGRANGIANS AND POTENTIALS

The effective Lagrangians are built under the heavy quark symmetry and SU(3)-flavor symmetry. The concrete expressions of the OBE Lagrangians read as

$$\mathcal{L}_B = \mathcal{L}_{B_3} + \mathcal{L}_S + \mathcal{L}_{int}, \quad (6)$$

$$\mathcal{L}_{B_3} = \frac{1}{2} \langle \bar{B}_3 (i v \cdot D) B_3 \rangle + i \beta_B \langle \bar{B}_3 v^\mu (\Gamma_\mu - V_\mu) B_3 \rangle + l_B \langle \bar{B}_3 \sigma B_3 \rangle, \quad (7)$$

$$\begin{aligned} \mathcal{L}_S = & - \langle \bar{S}^\alpha (i v \cdot D - \Delta_B) S_\alpha \rangle + \frac{3}{2} g_1 \langle i v_k \epsilon^{\mu\nu\lambda\kappa} \langle \bar{S}_\mu \mathbb{A}_\nu S_\lambda \rangle + i \beta_S \langle \bar{S}_\mu v_\alpha (\Gamma^\alpha - V^\alpha) S_\mu \rangle \\ & + \lambda_S \langle \bar{S}_\mu F^{\mu\nu} S_\nu \rangle + l_S \langle \bar{S}_\mu \sigma S_\mu \rangle, \end{aligned} \quad (8)$$

$$\mathcal{L}_{int} = g_4 \langle \bar{S}^\mu \mathbb{A}_\mu B_3 \rangle + i \lambda_I \epsilon^{\mu\nu\lambda\kappa} v_\mu \langle \bar{S}_\nu F^{\lambda\kappa} B_3 \rangle + h.c.. \quad (9)$$

The S^μ and B_3 are the heavy sextet and anti-triplet baryon superfield, defined as

$$S_\mu = B_\mu^* - \frac{1}{\sqrt{3}} (\gamma_\mu + v_\mu) \gamma^5 B_6. \quad (10)$$

These heavy baryon fields are

$$\begin{aligned} B_3 = & \begin{pmatrix} 0 & \Lambda_Q & \Xi_Q^{+1/2} \\ -\Lambda_Q & 0 & \Xi_Q^{-1/2} \\ \Xi_Q^{+1/2} & \Xi_Q^{-1/2} & 0 \end{pmatrix}, B_6 = \begin{pmatrix} \Sigma_Q^{+1} & \frac{1}{\sqrt{2}} \Sigma_Q^0 & \frac{1}{\sqrt{2}} \Xi_Q'^{+1/2} \\ \frac{1}{\sqrt{2}} \Sigma_Q^0 & \Sigma_Q^{-1} & \frac{1}{\sqrt{2}} \Xi_Q'^{-1/2} \\ \frac{1}{\sqrt{2}} \Xi_Q'^{+1/2} & \frac{1}{\sqrt{2}} \Xi_Q'^{-1/2} & \Omega_Q \end{pmatrix}, \\ B_6^* = & \begin{pmatrix} \Sigma_Q^{*+1} & \frac{1}{\sqrt{2}} \Sigma_Q^{*0} & \frac{1}{\sqrt{2}} \Xi_Q^{*'+1/2} \\ \frac{1}{\sqrt{2}} \Sigma_Q^{*0} & \Sigma_Q^{*-1} & \frac{1}{\sqrt{2}} \Xi_Q^{*-1/2} \\ \frac{1}{\sqrt{2}} \Xi_Q^{*'+1/2} & \frac{1}{\sqrt{2}} \Xi_Q^{*-1/2} & \Omega_Q^* \end{pmatrix}. \end{aligned} \quad (11)$$

The light meson part are given below

$$\begin{aligned} \mathbb{A} = & \frac{i}{2} [\xi^\dagger (\partial_\mu \xi) + (\partial_\mu \xi) \xi^\dagger], \quad \Gamma_\mu = \frac{1}{2} [\xi^\dagger (\partial_\mu \xi) - (\partial_\mu \xi) \xi^\dagger], \quad F_{\mu\nu} = \partial_\mu V_\nu - \partial_\nu V_\mu + [V_\mu, V_\nu], \\ \xi = & \exp\left[\frac{i\mathcal{M}}{f_\pi}\right], \\ \xi = & \begin{pmatrix} \frac{\pi^0}{\sqrt{2}} + \frac{\eta}{\sqrt{6}} & \pi^+ & K^+ \\ \pi^- & \frac{\pi^0}{\sqrt{2}} + \frac{\eta}{\sqrt{6}} & K^0 \\ K^- & \bar{K}^0 & -\frac{2}{\sqrt{6}}\eta \end{pmatrix}, \quad V^\mu = i \frac{g_V}{\sqrt{2}} \begin{pmatrix} \frac{\rho^0}{\sqrt{2}} + \frac{\omega}{\sqrt{2}} & \rho^+ & K^{*+} \\ \rho^- & -\frac{\rho^0}{\sqrt{2}} + \frac{\eta}{\sqrt{2}} & K^{*0} \\ K^{*-} & \bar{K}^{*0} & \phi \end{pmatrix}. \end{aligned} \quad (12)$$

For the pion decay constant, we use $f_\pi = 132$ MeV. As for the other coupling constants, we adopt the values in Ref. [22]:

$$\begin{aligned} g_2 = & -0.598, \quad g_4 = 0.999, \quad g_1 = \frac{8}{3} g_4, \\ g_3 = & \sqrt{\frac{2}{3}} g_4, \quad g_5 = -\sqrt{2} g_4, \quad g_A = 1.25, \\ l_B = & -3.1, \quad l_S = -2l_B, \quad \beta_B g_V = -6.0, \\ \beta_S g_V = & -2\beta_S g_V, \quad \lambda_S g_V = 19.2 \text{ GeV}^{-1}, \quad \lambda_I g_V = -\lambda_S g_V / \sqrt{8}. \end{aligned} \quad (13)$$

To get the effective potentials, we add a monopole form factor at each vertex

$$F_i(q) = \frac{\Lambda_i^2 - m_i^2}{\Lambda_i^2 - q^2}, \quad (14)$$

where the i stands for one of the propagators (π , η , σ , ρ and ω), the $q^2 = q_0^2 - \mathbf{q}^2$, and the Λ_i and m_i are the cutoff parameter and the mass of the corresponding propagator. After the Fourier transformation

$$V_i(r) = \frac{1}{(2\pi)^3} \int d\mathbf{q}^3 e^{-i\mathbf{q} \cdot \mathbf{r}} V(\mathbf{q}) F_i^2(q), \quad (15)$$

we can get the coordinate space potentials

$$\begin{aligned} V^{\Lambda_c \Sigma_c \rightarrow \Lambda_c \Sigma_c} &= -\frac{g_2^2}{f_\pi^2} \left[S(\boldsymbol{\sigma}_1, \boldsymbol{\sigma}_2) Y_3(\Lambda_\pi, q_0^C, m_\pi, r) + T(\boldsymbol{\sigma}_1, \boldsymbol{\sigma}_2) H_3(\Lambda_\pi, q_0^C, m_\pi, r) \right] \boldsymbol{\epsilon}_3^\dagger \cdot \boldsymbol{\epsilon}_2 + 2l_B l_S Y_0(\Lambda_\sigma, q_0, m_\sigma, r) \\ &\quad - \frac{1}{3} (\lambda_I g_V)^2 \left[2S(\boldsymbol{\sigma}_1, \boldsymbol{\sigma}_2) Y_3(\Lambda_\rho, q_0^C, m_\rho, r) - T(\boldsymbol{\sigma}_1, \boldsymbol{\sigma}_2) H_3(\Lambda_\rho, q_0^C, m_\rho, r) \right] \boldsymbol{\epsilon}_3^\dagger \cdot \boldsymbol{\epsilon}_2 \\ &\quad - \frac{1}{2} (\beta_B \beta_S g_V^2) Y_0(\Lambda_\omega, q_0, m_\omega, r), \end{aligned} \quad (16)$$

$$\begin{aligned} V^{\Lambda_c \Sigma_c^* \rightarrow \Lambda_c \Sigma_c^*} &= -\frac{g_4^2}{f_\pi^2} \left[S(\mathbf{S}_{t3}^\dagger, \mathbf{S}_{t2}) Y_3(\Lambda_\pi, q_0^C, m_\pi, r) + T(\mathbf{S}_{t3}^\dagger, \mathbf{S}_{t2}) H_3(\Lambda_\pi, q_0^C, m_\pi, r) \right] \boldsymbol{\epsilon}_3^\dagger \cdot \boldsymbol{\epsilon}_2 + 2l_B l_S Y_0(\Lambda_\sigma, q_0, m_\sigma, r) \\ &\quad + 2(\lambda_I g_V)^2 \left[2S(\mathbf{S}_{t3}^\dagger, \mathbf{S}_{t2}) Y_3(\Lambda_\rho, q_0^C, m_\rho, r) - T(\mathbf{S}_{t3}^\dagger, \mathbf{S}_{t2}) H_3(\Lambda_\rho, q_0^C, m_\rho, r) \right] \boldsymbol{\epsilon}_3^\dagger \cdot \boldsymbol{\epsilon}_2 \\ &\quad + \frac{1}{2} (\beta_B \beta_S g_V^2) Y_0(\Lambda_\omega, q_0, m_\omega, r), \end{aligned} \quad (17)$$

$$\begin{aligned} V^{\Sigma_c \Sigma_c \rightarrow \Sigma_c \Sigma_c} &= \frac{g_1^2}{2f_\pi^2} [S(\boldsymbol{\sigma}_1, \boldsymbol{\sigma}_2) Y_3(\Lambda_\pi, q_0, m_\pi, r) + T(\boldsymbol{\sigma}_1, \boldsymbol{\sigma}_2) H_3(\Lambda_\pi, q_0, m_\pi, r)] \mathbf{I}_1 \cdot \mathbf{I}_2 \\ &\quad + \frac{1}{3} \frac{g_1^2}{2f_\pi^2} [S(\boldsymbol{\sigma}_1, \boldsymbol{\sigma}_2) Y_3(\Lambda_\eta, q_0, m_\eta, r) + T(\boldsymbol{\sigma}_1, \boldsymbol{\sigma}_2) H_3(\Lambda_\eta, q_0, m_\eta, r)] - l_S^2 Y_0(\Lambda_\sigma, q_0, m_\sigma, r) \\ &\quad + \frac{1}{2} (g_S g_V)^2 Y_0(\Lambda_\rho, q_0, m_\rho, r) \mathbf{I}_1 \cdot \mathbf{I}_2 - \frac{1}{3} (\lambda_S g_V)^2 [2S(\boldsymbol{\sigma}_1, \boldsymbol{\sigma}_2) Y_3(\Lambda_\rho, q_0, m_\rho, r) - T(\boldsymbol{\sigma}_1, \boldsymbol{\sigma}_2) H_3(\Lambda_\rho, q_0, m_\rho, r)] \mathbf{I}_1 \cdot \mathbf{I}_2 \\ &\quad + \frac{1}{2} (\beta_S g_V)^2 Y_0(\Lambda_\omega, q_0, m_\omega, r) - \frac{1}{3} (\lambda_S g_V)^2 [2S(\boldsymbol{\sigma}_1, \boldsymbol{\sigma}_2) Y_3(\Lambda_\omega, q_0, m_\omega, r) - T(\boldsymbol{\sigma}_1, \boldsymbol{\sigma}_2) H_3(\Lambda_\omega, q_0, m_\omega, r)], \end{aligned} \quad (18)$$

$$\begin{aligned} V^{\Lambda_c \Sigma_c \rightarrow \Lambda_c \Sigma_c^*} &= -\frac{g_2 g_4}{f_\pi^2} \left[S(\mathbf{S}_{t3}^\dagger, \boldsymbol{\sigma}_2) Y_3(\Lambda_\pi, q_0^C, m_\pi, r) + T(\mathbf{S}_{t3}^\dagger, \boldsymbol{\sigma}_2) H_3(\Lambda_\pi, q_0^C, m_\pi, r) \right] \boldsymbol{\epsilon}_3^\dagger \cdot \boldsymbol{\epsilon}_2 \\ &\quad + \frac{2}{\sqrt{3}} (\lambda_I g_V)^2 \left[2S(\mathbf{S}_{t3}^\dagger, \boldsymbol{\sigma}_2) Y_3(\Lambda_\rho, q_0^C, m_\rho, r) - T(\mathbf{S}_{t3}^\dagger, \boldsymbol{\sigma}_2) H_3(\Lambda_\rho, q_0^C, m_\rho, r) \right] \boldsymbol{\epsilon}_3^\dagger \cdot \boldsymbol{\epsilon}_2, \end{aligned} \quad (19)$$

$$\begin{aligned} V^{\Lambda_c \Sigma_c \rightarrow \Sigma_c \Sigma_c} &= \frac{g_1 g_2}{\sqrt{2} f_\pi^2} [S(\boldsymbol{\sigma}_1, \boldsymbol{\sigma}_2) Y_3(\Lambda_\pi, q_0, m_\pi, r) + T(\boldsymbol{\sigma}_1, \boldsymbol{\sigma}_2) H_3(\Lambda_\pi, q_0, m_\pi, r)] \boldsymbol{\epsilon}_3^\dagger \cdot \mathbf{I}_2 \\ &\quad + \frac{2}{3\sqrt{6}} (\lambda_I \lambda_S g_V^2) \left[2S(\boldsymbol{\sigma}_1, \boldsymbol{\sigma}_2) Y_3(\Lambda_\rho, q_0, m_\rho, r) - T(\boldsymbol{\sigma}_1^\dagger, \boldsymbol{\sigma}_2) H_3(\Lambda_\rho, q_0, m_\rho, r) \right] \boldsymbol{\epsilon}_3^\dagger \cdot \mathbf{I}_2, \end{aligned} \quad (20)$$

$$\begin{aligned} V^{\Lambda_c \Sigma_c^* \rightarrow \Sigma_c \Sigma_c} &= \frac{g_2 g_3}{\sqrt{2} f_\pi^2} [S(\boldsymbol{\sigma}_1, \mathbf{S}_{t2}) Y_3(\Lambda_\pi, q_0, m_\pi, r) + T(\boldsymbol{\sigma}_1, \mathbf{S}_{t2}) H_3(\Lambda_\pi, q_0, m_\pi, r)] \boldsymbol{\epsilon}_3^\dagger \cdot \mathbf{I}_2 \\ &\quad - \frac{1}{3\sqrt{2}} (\lambda_I \lambda_S g_V^2) [2S(\boldsymbol{\sigma}_1, \mathbf{S}_{t2}) Y_3(\Lambda_\rho, q_0, m_\rho, r) - T(\boldsymbol{\sigma}_1, \mathbf{S}_{t2}) H_3(\Lambda_\rho, q_0, m_\rho, r)] \boldsymbol{\epsilon}_3^\dagger \cdot \mathbf{I}_2. \end{aligned} \quad (21)$$

$$(22)$$

We added a factor -1 for the cross-diagram potentials, which contain the q_0^C . The factor is from the fermions position exchange, and equal to $(-1)^{s-s_1-s_2+l+i-i_1-i_2+1}$, where the $s, s_1, s_2, l, i, i_1, i_2$ are spin, orbit and isospin numbers. The $\boldsymbol{\epsilon}$ and \mathbf{I} are the isospin polarization vector and isospin operator respectively, and the isospin-dependent matrix elements are given in Table V. The \mathbf{S}_t and $\boldsymbol{\sigma}$ are the spin transition operator and Pauli operator respectively. The spin-dependent operators have $S(\mathbf{a}, \mathbf{b}) = \mathbf{a} \cdot \mathbf{b}$ and $T(\mathbf{a}, \mathbf{b}) = 3(\mathbf{a} \cdot \mathbf{r})(\mathbf{b} \cdot \mathbf{r})/r^2 - \mathbf{a} \cdot \mathbf{b}$, whose matrix elements are given

in Table IV. The Y_3 , H_3 functions and relevant Y , H functions are defined as

$$\begin{aligned}
Y(x) &= \frac{e^{-x}}{x}, \quad H(x) = (1 + \frac{3}{x} + \frac{3}{x^2})Y(x), \\
Y_0(\Lambda, q_0, m, r) &= \frac{u}{4\pi} [Y(ur) - \frac{\chi}{u} Y(\chi r) - \frac{\beta^2}{2\chi u} e^{-\chi r}], \\
Y_3(\Lambda, q_0, m, r) &= \frac{u^3}{12\pi} [Y(ur) - \frac{\chi}{u} Y(\chi r) - \frac{\beta^2 \chi}{2u^3} e^{-\chi r}], \\
H_3(\Lambda, q_0, m, r) &= \frac{u^3}{12\pi} [H(ur) - (\frac{\chi}{u})^3 H(\chi r) \\
&\quad - \frac{\beta^2}{2\chi u} \frac{\chi^2}{u^2} Y(\chi r) - \frac{\beta^2}{2\chi u} \frac{\chi^2}{u^2} e^{-\chi r}],
\end{aligned} \tag{23}$$

where the

$$\begin{aligned}
u &= \text{Sign}[\text{Re}(e^{i\theta} \sqrt{m^2 - q_0^2})] \sqrt{m^2 - q_0^2}, \\
\beta &= \sqrt{\Lambda^2 - m^2}, \quad \chi = \sqrt{\Lambda^2 - q_0^2}.
\end{aligned} \tag{24}$$

TABLE IV: The spin-dependent matrix elements.

Δ	$S(\sigma_1^\dagger, \sigma_2)$	$T(\sigma_1^\dagger, \sigma_2)$	$S(\mathbf{S}_{t3}^\dagger, \mathbf{S}_{t2})$	$T(\mathbf{S}_{t3}^\dagger, \mathbf{S}_{t2})$	$S(\mathbf{S}_{t3}^\dagger, \sigma_2)$	$T(\mathbf{S}_{t3}^\dagger, \sigma_2)$	$S(\sigma_1, \mathbf{S}_{t2})$	$T(\sigma_1, \mathbf{S}_{t2})$
$\langle {}^3S_1 \Delta {}^3S_1 \rangle$	1	0	$\frac{1}{3}$	0	$-2\sqrt{\frac{2}{3}}$	0	$2\sqrt{\frac{2}{3}}$	0
$\langle {}^3D_1 \Delta {}^3S_1 \rangle$	0	$2\sqrt{2}$	0	$-\frac{5}{3\sqrt{2}}$	0	$\frac{1}{\sqrt{3}}$	0	$-\frac{1}{\sqrt{3}}$
$\langle {}^3S_1 \Delta {}^3D_1 \rangle$	0	$2\sqrt{2}$	0	$-\frac{5}{3\sqrt{2}}$	0	$\frac{1}{\sqrt{3}}$	0	$-\frac{1}{\sqrt{3}}$
$\langle {}^3D_1 \Delta {}^3D_1 \rangle$	1	-2	$\frac{1}{3}$	$\frac{5}{6}$	$-2\sqrt{\frac{2}{3}}$	$-\frac{1}{\sqrt{6}}$	$2\sqrt{\frac{2}{3}}$	$\frac{1}{\sqrt{6}}$
Δ	$S(\sigma_1^\dagger, \sigma_2)$							
$\langle {}^1S_0 \Delta {}^1S_0 \rangle$	-3							

TABLE V: The isospin-dependent ($I=1$) matrix elements of the operators $\epsilon_3^\dagger \cdot \epsilon_2$, $\epsilon_3^\dagger \cdot \mathbf{I}_2$ and $\mathbf{I}_1 \cdot \mathbf{I}_2$.

Δ	$\epsilon_3^\dagger \cdot \epsilon_2$	$\epsilon_3^\dagger \cdot \mathbf{I}_2$	$\mathbf{I}_1 \cdot \mathbf{I}_2$
$\langle I=1 \Delta I=1 \rangle$	1	$-\sqrt{2}$	-1

IV. NUMERICAL RESULTS

A. The OPE potential results for the double-charm hexaquark system

We first introduce the OPE potentials to study the double-charm hexaquark system. For the $1(0^+)$ system, we do not get a bound or resonant state with a reasonable cutoff Λ_π . However, we find a quasibound state in the $1(1^+)$ case, and the results are shown in row "Adopt" of Table VI. One could find this pole has an imaginary part corresponding to $-i\Gamma/2$. We give a brief explanation of the measure $\langle \tilde{\psi}_i | \psi_i \rangle$ herein. The $\langle \tilde{\psi}_i | \psi_i \rangle = e^{i\theta} \int_0^\infty \{\psi_i(re^{i\theta})\}^2 dr$ is the amplitude corresponding to the i -th channel. This measure is similar to the definition of the probabilities of bound states. However, one could find that its value could be complex in Table VI and could not be regarded as probabilities. This behavior is from the normalization of the resonance wave function [69, 71]. However, the quasibound state herein is special. When the bound energy $B.E. \leq -(m_{\Sigma_c} - m_{\Lambda_c} - m_\pi)$, the quasibound state turns into a bound state, and the width from the three-body decay effect vanishes. Then the $\langle \tilde{\psi}_i | \psi_i \rangle$ turns into the probability of the i -th channel. Hence this measure could partly reflect the constituents of this special quasibound state. Furthermore, the $\sqrt{\langle r^2 \rangle}$ is the root-mean-square-radius. Its real part is interpreted as an expectation value, and the imaginary part corresponds to a measure of the uncertainty in observation [72].

To make a comparison, we also give the result under the instantaneous approximation in row " $q_0 = 0$ " of Table VI. In this case, the imaginary part of the OPE potential from the three-body decay effect disappears, and the pole becomes a bound state. Considering the cases in row "Adopt" with $\Lambda_\pi = 1.0$ and row " $q_0 = 0$ " with $\Lambda_\pi = 1.05$, we find their values are close to each other, including the energy, $\sqrt{\langle r^2 \rangle}$ and $\langle \tilde{\psi}_i | \psi_i \rangle$. In fact, we find this conclusion could extend to other similar systems. In other words, the influence of the three-body decay is small. Therefore, we will take the $\sqrt{\langle r^2 \rangle}$ and $\langle \tilde{\psi}_i | \psi_i \rangle$ as the reference measures when analyzing the size and constituents of the pole state.

	Λ_π (GeV)	1.0	1.05	1.1
Adopt	Energy (MeV)	$-5.61 - 0.43i$	$-13.90 - 0.29i$	$-25.57 - 0.04i$
	$\sqrt{\langle r^2 \rangle}$ (fm)	$1.4 - 0.1i$	0.9	0.7
	$\langle \tilde{\psi}_i \psi_i \rangle \times 100$	$(70.7 - 1.4i/1.7/23.9 + 1.3i/0.9/2.5 + 0.1i/0.3)$	$(59.0 - 0.4i/1.2/34.1 + 0.4/1.2/4.2/0.3)$	$(50.8/0.8/40.8/1.4/6.0/0.3)$
$q_0 = 0$	Energy (MeV)	-0.54	-5.64	-16.51
	$\sqrt{\langle r^2 \rangle}$ (fm)	4.1	1.3	0.8
	$\langle \tilde{\psi}_i \psi_i \rangle \times 100$	$(91.4/1.0/6.4/0.3/0.7/0.2)$	$(71.7/1.2/22.8/0.8/3.1/0.4)$	$(56.8/0.8/35.4/1.2/5.5/0.3)$

TABLE VI: Solutions for the double-charm hexaquark with $I(J^P) = 1(1^+)$ in the OPE potential case with the $\theta = 20^\circ$. The energies are given relative to the threshold of $\Lambda_c \Sigma_c$. The $\sqrt{\langle r^2 \rangle} = [e^{3i\theta} \int_0^\infty \{\psi(re^{i\theta})\}^2 r^2 dr]^{1/2}$ is the root-mean-square (RMS) radius. The $\langle \tilde{\psi}_i | \psi_i \rangle = e^{i\theta} \int_0^\infty \{\psi_i(re^{i\theta})\}^2 dr$ is the amplitude corresponding to the i -th channel of $\Lambda_c \Sigma_c(^3S_1, ^3D_1)$, $\Lambda_c \Sigma_c^*(^3S_1, ^3D_1)$, $\Sigma_c \Sigma_c(^3S_1, ^3D_1)$. The data of the row "Adopt" are the results we actually adopt, and the q_0 herein is from Table III. The data of row " $q_0 = 0$ " are from the instantaneous approximation.

In our framework, the width of a quasibound state should not be larger than the value of Σ_c and will decrease as the binding energy becomes deeper. In fact, so it does. Taking the case $\Lambda_\pi = 1.0$ GeV as an example, we get a quasibound state whose binding energy and width are -5.61 MeV and 0.86 MeV respectively. And its dominant constituents are S -wave $\Lambda_c \Sigma_c$ and $\Lambda_c \Sigma_c^*$. In fact, the main channel $\Lambda_c \Sigma_c(^3S_1)$ contributes a repulsive potential, and the $\Lambda_c \Sigma_c^*(^3S_1)$ contributes an attractive potential with an imaginary part. Considering only the former channel, one could not get a bound state. However, one could get a quasibound state when adding the attractive potential of channel $\Lambda_c \Sigma_c^*$. Obviously, the coupled-channel effects play an important role in this system. To gain a deeper insight, we would add the other medium- and short-range potentials in the following parts.

B. The OBE potential results for the double-charm hexaquark system

In this part, we further employ the OBE potential to include the short- and medium-range contribution. Before making a calculation, we need to choose the cutoff for the different vertex first. The same cutoff is usually used for all the OBE potentials, like $\Lambda_\pi = \Lambda_\eta = \Lambda_\sigma = \Lambda_\rho = \Lambda_\omega$ (common cutoff). Another possible choice could be found in Refs. [73, 74]. The authors adopted $\Lambda_i = m_i + \alpha \Lambda_{\text{QCD}}$ (scaled cutoff), where the i is corresponds to a propagator ($\pi, \eta, \sigma, \rho, \omega$), $\Lambda_{\text{QCD}} = 220$ MeV is the scale of QCD, and α is a dimensionless parameter. However, these two choices could both be invalid in this work.

As shown in Table VI, the cutoff in the OPE potential case is close to 1 GeV. And when we add the other potentials from the OBE interaction and adopt the common cutoff, the reasonable value is around $\Lambda_i \approx 0.8$ GeV. Then a problem emerges. Since the $m_\rho/m_\omega \approx 0.78$ GeV, their form factors $F_i(q) = (\Lambda_i^2 - m_i^2)/(\Lambda_i^2 - q^2) \rightarrow 0$, and then the short-range ρ, ω potentials go to 0. On the other hand, if we adopt the scaled cutoff scheme, the ρ, ω potentials could be much larger than the π potential. It may also be doubtful since the OPE potential should play a more important role than the one-vector-exchange (OVE) potentials for the state very close to the thresholds. To deal with this problem, we adopt a compromise scheme—assuming $\Lambda_i = m_i [1 + \alpha(\Lambda_{\text{QCD}}/m_i)^2]$.

Adopting the compromise scheme for the cutoff, we get the results in the OBE potential case for the $1(1^+)$ system in Table VII. We find a quasibound state, and its behavior is just like the situation in the OPE potential case.

We take the $\alpha = 2.2$ as an example and show the eigenvalue distribution in the OBE potential case, as shown in Fig. 3. Obviously, the quasibound state pole is located on the first Riemann sheets (physical sheets) corresponding to the $\Lambda_c \Sigma_c, \Lambda_c \Sigma_c^*$ and $\Sigma_c \Sigma_c$ channels and the second Riemann sheets (unphysical sheets) corresponding to the $\Lambda_c \Lambda_c \pi$ three-body channel. In Fig. 4, we choose $\theta = 20^\circ$ and plot the real and imaginary parts of its wave function. Obviously, the S -wave $\Lambda_c \Sigma_c$ and $\Lambda_c \Sigma_c^*$ channels dominate the state.

α	2.0	2.2	2.4
Energy (MeV)	$-3.98 - 0.31i$	$-14.27 - 0.25i$	-31.06
$\sqrt{\langle r^2 \rangle}$ (fm)	$1.7 - 0.1i$	1.0	0.7
$\langle \tilde{\psi}_i \psi_i \rangle \times 100$	$(81.6 - 1.5i / 1.7 / 14.8 + 1.4i / 0.5 / 1.2 + 0.1i / 0.2)$	$(66.5 - 0.4i / 1.1 / 28.2 + 0.4i / 0.8 / 3.1 / 0.2)$	$(55.5 / 0.7 / 37.3 / 1.1 / 5.3 / 0.2)$

TABLE VII: Solutions for the double-charm hexaquark with $I(J^P) = 1(1^+)$ in the OBE potential case with the $\theta = 20^\circ$. The energies are given relative to the threshold of $\Lambda_c \Sigma_c$. The $\sqrt{\langle r^2 \rangle} = [e^{3i\theta} \int_0^\infty \{\psi(re^{i\theta})\}^2 r^2 dr]^{1/2}$ is the root-mean-square (RMS) radius. The $\langle \tilde{\psi}_i | \psi_i \rangle = e^{i\theta} \int_0^\infty \{\psi_i(re^{i\theta})\}^2 dr$ is the amplitude corresponding to the i -th channel of $\Lambda_c \Sigma_c(^3S_1, ^3D_1)$, $\Lambda_c \Sigma_c^*(^3S_1, ^3D_1)$, $\Sigma_c \Sigma_c(^3S_1, ^3D_1)$.

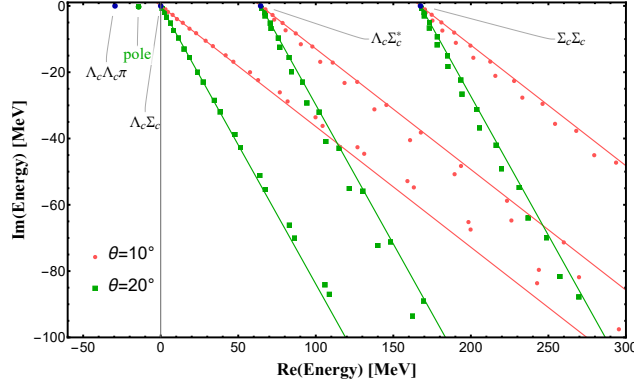


FIG. 3: The eigenvalue distribution of the double-charm hexaquark with the $I(J^P) = 1(1^+)$. The $\alpha = 2.2$ in the OBE potential case. The red (green) points (square point) and lines correspond to the situation with the complex rotation angle $\theta = 10^\circ (20^\circ)$.

C. The OBE potential results for the hidden-charm hexaquark system

In this part, we discuss the molecule system of the hidden-charm hexaquark with the OBE potential. The relevant potentials are similar to those of the double-charm cases, and they could be connected by making a G parity transformation for the propagators. In other words,

$$V^{AB} = (-1)^{G_i} V^{A\bar{B}}, \quad (25)$$

where the A, B are the charmed baryons, and G_i is the G parity of the i propagator, as shown in Table VIII.

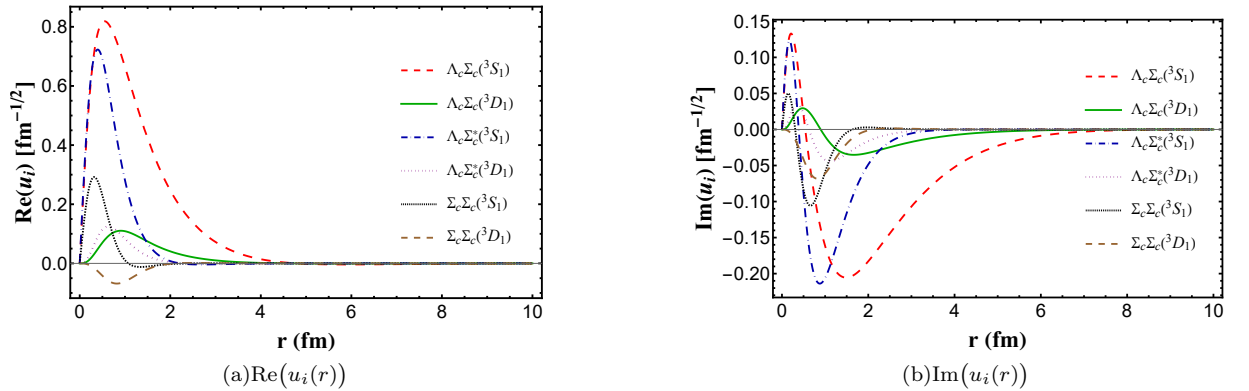


FIG. 4: The wave functions $u_i(r)$ ($i = 1, 2, 3, 4, 5, 6$) of the double-charm hexaquark with the $I(J^P) = 1(1^+)$. The rotation angle $\theta = 20^\circ$ and the parameter $\alpha = 2.2$ in the OBE potential case. The two diagrams correspond to: (a) the real part of the $u_i(r)$ (b) the imaginary part of the $u_i(r)$.

TABLE VIII: G parity of the light mesons.

Meson	π	η	σ	ρ	ω
G	-1	1	1	1	-1

Considering the multichannel coupling effect, we adopt the channels in Table I for the systems $1^+(0^{--})$, $1^-(0^{-+})$, $1^+(1^{--})$ and $1^-(1^{-+})$. Compared with the double-charm case, the number of the hidden-charm systems doubles for the existence of the C or G parity number. For the $1^-(0^{-+})$ case, we do not find a pole in a reasonable cutoff region. For the positive G parity case $1^+(0^{--})$, we find a quasibound state, and the results are given in Table IX. This system has only one channel, and one may find a clearer width behavior than in the other coupled-channel systems. When the $\alpha = 1.5$, we find a quasibound state with the binding energy of -5.37 MeV, and the width of 1.72 MeV. Obviously, the width is very close to the upper limit of this pole—the width of the Σ_c .

α	1.5	1.8	2.1
Energy (MeV)	-5.37 - 0.86i	-13.29 - 0.46i	-25.63 - 0.05i
$\sqrt{\langle r^2 \rangle}$ (fm)	1.7	1.2	0.9

TABLE IX: Solutions for the hidden-charm hexaquark with $I^G(J^{PC}) = 1^+(0^{--})$ in the OBE potential case with the $\theta = 20^\circ$. The energies are given relative to the threshold of $\Lambda_c \bar{\Sigma}_c$. The $\sqrt{\langle r^2 \rangle} = [e^{3i\theta} \int_0^\infty \{\psi(re^{i\theta})\}^2 r^2 dr]^{1/2}$ is the root-mean-square (RMS) radius.

For the vector cases, both the $1^+(1^{--})$ and $1^-(1^{-+})$ systems can form a quasibound state. We first discuss the $1^-(1^{-+})$ system. Similar to the double-charm case $1(1^+)$, the first diagonal S -wave OPE potential $V_\pi^{\{\Lambda_c \bar{\Sigma}_c\} \rightarrow \{\Lambda_c \bar{\Sigma}_c\}}$ is repulsive, and the third diagonal S -wave OPE potential $V_\pi^{[\Lambda_c \bar{\Sigma}_c^*] \rightarrow [\Lambda_c \bar{\Sigma}_c^*]}$ is attractive. The numerical results of this pole are given in Table X, and the main contributions are from the S -wave channels $\{\Lambda_c \bar{\Sigma}_c\}$ and $[\Lambda_c \bar{\Sigma}_c^*]$. In fact, this quasibound state is very similar to the pole in the double-charm case $1(1^+)$. They have very similar results with the same energy, including the widths, constituents and sizes. For example, taking the $\alpha = 2.03$, we get the binding energy of -4.21 MeV, the width of 0.56 MeV, the RMS of 1.7-0.1i fm and $\langle \psi_i | \psi_i \rangle \times 100 = (83.8 - 1.3i / 2.5 / 13.2 + 1.3i / 0.5)$, which are very similar to the results in Table VI with $\alpha = 2.0$.

α	2.1	2.3	2.5
Energy (MeV)	-6.43 - 0.32i	-15.33 - 0.23i	-27.88 - 0.01i
$\sqrt{\langle r^2 \rangle}$ (fm)	1.5	1.0	0.8
$\langle \psi_i \psi_i \rangle \times 100$	(80.0 - 1.1i / 2.5 / 17.0 + 1.1i / 0.6)	(69.7 - 0.4i / 2.3 / 27.1 + 0.4i / 0.9)	(61.2 / 2.2 / 35.4 / 1.2)

TABLE X: Solutions for the hidden-charm hexaquark with $I^G(J^{PC}) = 1^-(1^{-+})$ in the OBE potential case with the $\theta = 20^\circ$. The energies are given relative to the threshold of $\Lambda_c \bar{\Sigma}_c$. The $\sqrt{\langle r^2 \rangle} = [e^{3i\theta} \int_0^\infty \{\psi(re^{i\theta})\}^2 r^2 dr]^{1/2}$ is the root-mean-square (RMS) radius. The $\langle \psi_i | \psi_i \rangle = e^{i\theta} \int_0^\infty \{\psi_i(re^{i\theta})\}^2 dr$ is the amplitude corresponding to the i -th channel of $\{\Lambda_c \bar{\Sigma}_c\} (^3S_1, ^3D_1)$, $[\Lambda_c \bar{\Sigma}_c^*] (^3S_1, ^3D_1)$.

Then, we consider the $1^+(1^{--})$ case. Contrary to the $1^-(1^{-+})$, the first diagonal S -wave OPE potential $V_\pi^{[\Lambda_c \bar{\Sigma}_c] \rightarrow [\Lambda_c \bar{\Sigma}_c]}$ is attractive, and the third diagonal S -wave OPE potential $V_\pi^{\Lambda_c \bar{\Sigma}_c^* \rightarrow \Lambda_c \bar{\Sigma}_c^*}$ is repulsive. In other words, the first channel could form a bound or quasibound state alone. After considering the coupled-channel effect, we can obtain the solutions, as shown in Table XI. Different from the other cases, this system has two poles when $\alpha \gtrsim 1.9$. The first one is close to the threshold of the $\Lambda_c \bar{\Sigma}_c$, and the second to the $\Lambda_c \bar{\Sigma}_c^*$. These two poles are quite different.

To study their characters, we illustrate the energy distribution with the $\alpha = 1.9$ in Fig. 5. The first pole mainly consists of the S -wave $[\Lambda_c \bar{\Sigma}_c]$ with the energy of -15.37 - 0.23i MeV. It is located on the first Riemann sheets (physical sheets) corresponding to the channels $[\Lambda_c \bar{\Sigma}_c]$, $\{\Lambda_c \bar{\Sigma}_c^*\}$ and $\Sigma_c \bar{\Sigma}_c$, and the second Riemann sheets (unphysical sheets) corresponding to the three-body channel $\Lambda_c \bar{\Lambda}_c \pi$. The second pole mainly consists of the S -wave $\{\Lambda_c \bar{\Sigma}_c^*\}$ with the energy of 63.55 - 1.36i MeV relative to the threshold of $[\Lambda_c \bar{\Sigma}_c]$. It is located on the first Riemann sheets (physical sheets) corresponding to the channels $\{\Lambda_c \bar{\Sigma}_c^*\}$ and $\Sigma_c \bar{\Sigma}_c$, and the second Riemann sheets (unphysical sheets) corresponding to the $[\Lambda_c \bar{\Sigma}_c]$ and the $\Lambda_c \bar{\Lambda}_c \pi$ three-body channel. Obviously, the second pole is a Feshbach-type resonance—if we turn off the $\Lambda_c \bar{\Sigma}_c^*$ channels, it disappears. In addition, the width of the first pole is totally from the three-body decay process. However, the width of the second one may have additional sources.

To figure out this source, we take the instantaneous approximation $q_0 = 0$. We also obtain two similar poles that

pole	α	1.7	1.9	2.1
1	Energy (MeV)	$-7.28 - 0.45i$	$-15.37 - 0.23i$	-27.66
	$\sqrt{\langle r^2 \rangle}$ (fm)	1.5	1.1	0.9
	$\langle \tilde{\psi}_i \psi_i \rangle \times 100$	$(92.7 - 0.2i/3.0/2.9 + 0.2i/0./0.5/0.9)$	$(89.7 - 0.1i/3.5/3.8 + 0.1i/0./1.3/1.7)$	$(86.0/4.3/3.8/0./3.0/2.8)$
2	Energy (MeV)		$63.55 - 1.36i$	$53.95 - 3.25i$
	$\sqrt{\langle r^2 \rangle}$ (fm)		$2.5 - 0.7i$	$1.1 - 0.2i$
	$\langle \tilde{\psi}_i \psi_i \rangle \times 100$		$(-0.6i/-1.6 + 0.8i/91.4 - 9.9i/5.9 + 8.1i/4.1 + 1.6i/0.1 + 0.1i)$	$(-0.9/-0.6 + 9.9i/67.3 - 9.6i/3.9 - 1.1i/29.3 + 0.4i/1.0 + 0.3i)$
2I	Energy (MeV)		$63.66 - 1.45i$	$53.77 - 2.28i$
	$\sqrt{\langle r^2 \rangle}$ (fm)		$2.3 - 1.1i$	$1.1 - 0.1i$
	$\langle \tilde{\psi}_i \psi_i \rangle \times 100$		$(-0.6 - 0.5i/-1.1 + 1.5i/93.7 - 3.5i/2.1 + 0.4i/5.7 + 2.1i/0.1)$	$(0.7i/2.0 + 6.1i/72.5 - 4.9i/1.6 - 0.1i/23.4 - 1.8i/0.5)$

TABLE XI: Solutions for the hidden-charm hexaquark with $I^G(J^{PC}) = 1^+(1^{--})$ in the OBE potential case with the $\theta = 20^\circ$. The energies are given relative to the threshold of $\Lambda_c \bar{\Sigma}_c$. The $\sqrt{\langle r^2 \rangle} = [e^{3i\theta} \int_0^\infty \{\psi(re^{i\theta})\}^2 r^2 dr]^{1/2}$ is the root-mean-square (RMS) radius. The $\langle \tilde{\psi}_i | \psi_i \rangle = e^{i\theta} \int_0^\infty \{\psi_i(re^{i\theta})\}^2 dr$ is the amplitude corresponding to the i -th channel of $[\Lambda_c \bar{\Sigma}_c](^3S_1, ^3D_1)$, $\{\Lambda_c \bar{\Sigma}_c^*\}(^3S_1, ^3D_1)$, $\Sigma_c \bar{\Sigma}_c(^3S_1, ^3D_1)$. The data of row "2" are the results we actually adopt, and the q_0 herein is from Table III. The data of row "2I" are from the instantaneous approximation with $q_0 = 0$.

correspond to poles "1" and "2" in Table XI. The one corresponding to pole "1" turns into a bound state, and we have discussed this case in Sec. IV A. We will focus on the other pole, whose numerical results are listed in row "2I" of Table XI. Its energy becomes $63.66 - 1.45i$ MeV for the $\alpha = 1.9$ case, whose real part is nearly unchanged compared with "2" pole with energy of $63.55 - 1.36i$ MeV. However, its width changes and does not disappear like the other quasibound state. As discussed in the Sec. IV A, the width from the three-body decay will vanish under the instantaneous approximation. Therefore, the width in "2I" is totally from the two-body decay process, such as the decay of the pole "2I" $\rightarrow [\Lambda_c \bar{\Sigma}_c]$. We infer from the change of the width that the two-body decay plays a more important role than the three-body decay in this resonance.

Finally, we also plot the wave functions of poles "1" and "2", as shown in Fig. 6. We choose $\theta = 20^\circ$ and present the real and imaginary parts of their wave functions. Obviously, the S -wave $[\Lambda_c \bar{\Sigma}_c]$ and $\{\Lambda_c \bar{\Sigma}_c^*\}$ channels dominate the first pole, and S -wave $\{\Lambda_c \bar{\Sigma}_c^*\}$ channel dominate the second pole.

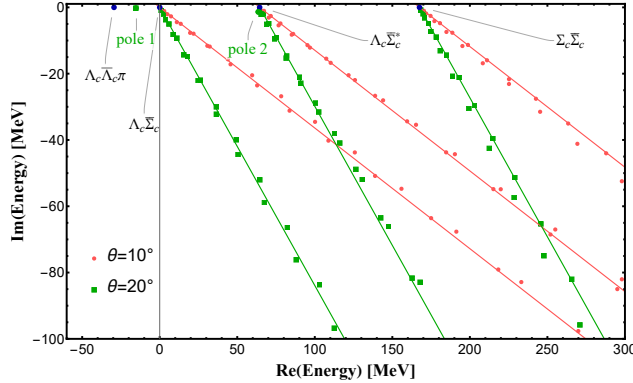


FIG. 5: The eigenvalue distribution of the hidden-charm hexaquark with the $I(J^P) = 1^+(1^{--})$. The $\alpha = 1.9$ in the OBE potential case. The red (green) points (square point) and lines correspond to the situation with the complex rotation angle $\theta = 10^\circ (20^\circ)$.

V. SUMMARY

In this work, we use the complex scaling method to study the double-charm and hidden-charm hexaquark states in the molecule picture. In order to include the coupled-channel effects, we consider the channels $\Lambda_c \Sigma_c^{(*)}$ (or $\Lambda_c \bar{\Sigma}_c^{(*)}$) and $\Sigma_c \Sigma_c$ (or $\Sigma_c \bar{\Sigma}_c$). We also take into account the $S - D$ wave mixing effect in this deuteronlike dibaryon (hidden-charm

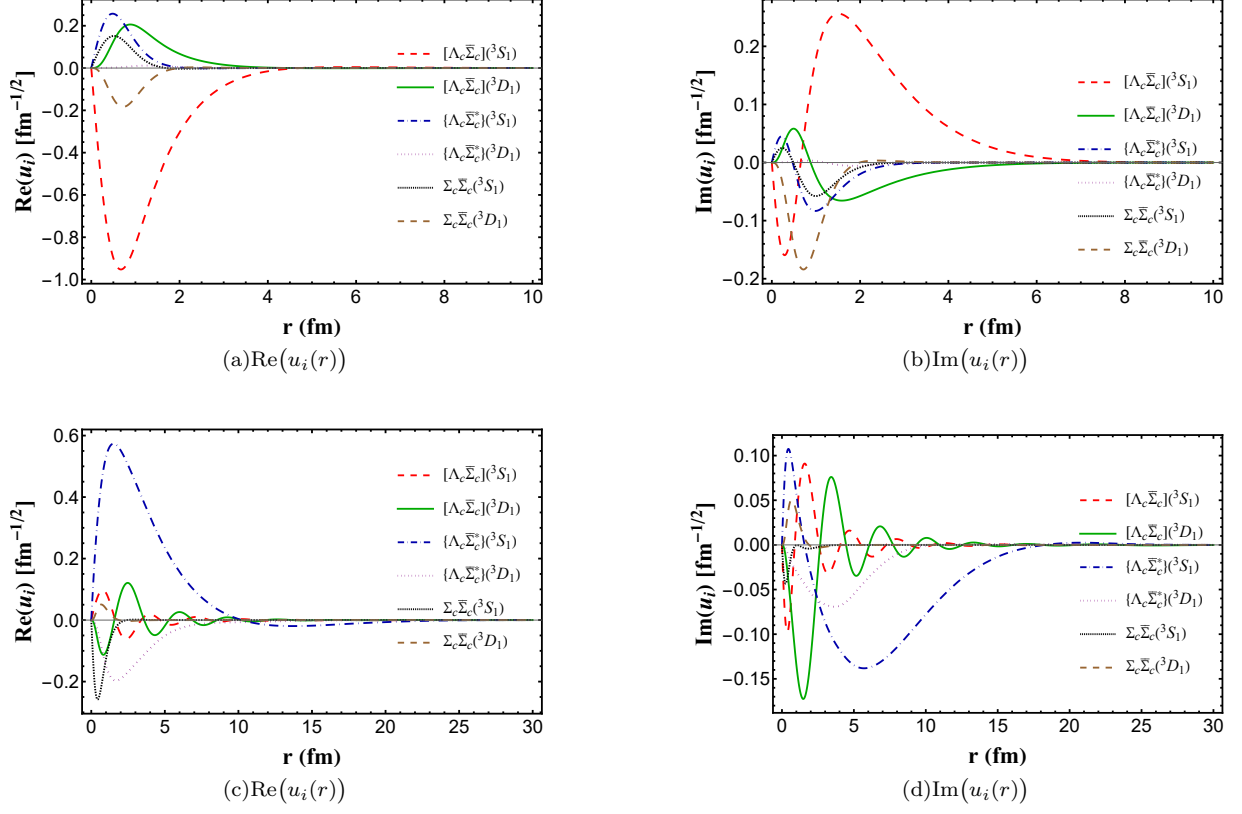


FIG. 6: The wave functions $u_i(r)$ ($i = 1, 2, 3, 4, 5, 6$) of the hidden-charm hexaquark with the $I(J^P) = 1^+(1^{--})$. The rotation angle $\theta = 20^\circ$ and the parameter $\alpha = 1.9$ in the OBE potential case. The four diagrams correspond to: (a) the real part of the $u_i(r)$ for the first pole (b) the imaginary part of the $u_i(r)$ for the first pole (c) the real part of the $u_i(r)$ for the second pole (d) the imaginary part of the $u_i(r)$ for the second pole.

baryonium), as shown in Table I.

We adopt the effective Lagrangians constructed in terms of the heavy quark symmetry and chiral symmetry. To figure out the influence of the long-range pion exchange in the formation of the bound states and resonances, we adopt the OPE potential for the double-charm hexaquark system. And we also give the numerical results with the OBE potential for the double-charm and hidden-charm hexaquark systems.

The OPE potentials of the $\Lambda_c \Sigma_c^{(*)}$ and the tetraquark DD^* systems are similar. They both have an imaginary part. This imaginary part comes from the processes $\Sigma_c^{(*)} \rightarrow \Lambda_c \pi$ ($D^* \rightarrow D \pi$), which can be naturally understood in the framework of the CSM. In the study of the double-charm hexaquark system with the OPE potential, we find a quasibound state in the $1(1^+)$ system, which mainly consists of the S -wave $\Lambda_c \Sigma_c$ and $\Lambda_c \Sigma_c^*$. When taking $\Lambda_\pi = 1$ GeV, the binding energy relative to the $\Lambda_c \Sigma_c$ is -5.6 MeV, and the width is 0.86 MeV. As explained in Sec. IV A, this width is totally from the $\Lambda_c \Lambda_c \pi$ three-body decay process. For the system with $1(0^+)$, we do not find a bound state or resonance.

We also employ the OBE potential to include the medium- and short-range interactions. And we get a similar result compared with the OPE case—only one pole is found. Its binding energy relative to the $\Lambda_c \Sigma_c$ and width are -14.27 MeV and 0.50 MeV respectively when taking the $\alpha = 2.2$. The S -wave $\Lambda_c \Sigma_c$ and $\Lambda_c \Sigma_c^*$ are the dominant constituents, and the D -wave constituents still provide small contributions.

For the hidden-charm hexaquark systems, we find more poles. In the $1^-(0^{++})$ case, we do not find a pole in a reasonable cutoff region. However, we find a quasibound state in the $1^+(0^{--})$ case with a single channel. When $\alpha = 1.5$, the binding energy is -5.37 MeV relative to the $\Lambda_c \bar{\Sigma}_c$ threshold. Its width is 1.72 MeV which is very close to the width of Σ_c . In the vector cases, we find poles in both the $1^+(1^{--})$ and $1^-(1^{++})$ cases. For the $1^-(1^{++})$ case, we find a quasibound state, which behaves just like the mentioned pole in the $1(1^+)$ double-charm hexaquark. We get this pole in similar region $\alpha \in [2.0 \sim 2.5]$. For the same energy or cutoff, their widths, sizes and constituents are close to each other too. For the $1^+(1^{--})$ case, we find two poles—a pole close to the $\Lambda_c \bar{\Sigma}_c$ threshold and the other close

to the $\Lambda_c \bar{\Sigma}_c^*$ threshold. Taking $\alpha = 1.9$, the first pole as a quasibound state has a binding energy of -15.37 MeV and a width of 0.46 MeV, and the S -wave $[\Lambda_c \bar{\Sigma}_c]$ plays a dominant role. The second pole is a resonance, whose energy relative to the $\Lambda_c \bar{\Sigma}_c$ threshold is $63.55 - 1.36i$ MeV. Different from the above quasibound states whose widths are totally from the three-body decay, its width arises from two sources—the three-body decay and the two-body decay. As shown in Table XI, its width does not vanish when we get rid of the three-body decay effect, and the contribution from the two-body decay is apparently larger. We also plot the wave functions of these two poles, see in Fig. 6.

In summary, we have found some quasibound states and resonances in these systems. One could look for these states through their strong decay patterns, such as $[\Lambda_c \bar{\Sigma}_c]$ and $\Lambda_c \bar{\Lambda}_c \pi$ invariant mass distributions in the hidden-charm baryonium and $\Lambda_c \Lambda_c \pi$ invariant mass distribution in the double-charm dibaryon. Especially, the $1^+(0^{--})$ and $1^-(1^{+-})$ hidden-charm hexaquark molecular states are very interesting. These isovector mesons have exotic J^{PC} quantum numbers which are not accessible to the conventional $q\bar{q}$ mesons. Hopefully, this work could be helpful for future experimental search of the hexaquark states at facilities such as LHCb and BelleII.

Acknowledgments

This research is supported by the National Science Foundation of China under Grants No. 11975033, No. 12070131001 and No. 12147168.

-
- [1] P. Adlarson and et al, *Phys. Rev. Lett.* **106**, 242302 (2011).
 - [2] P. Adlarson and et al, *Physics Letters B* **721**, 229 (2013).
 - [3] P. Adlarson and et al, *Phys. Rev. C* **88**, 055208 (2013).
 - [4] P. Adlarson and et al, *Phys. Rev. Lett.* **112**, 202301 (2014).
 - [5] M. Bashkanov and et al, *Phys. Rev. Lett.* **102**, 052301 (2009).
 - [6] R. L. Jaffe, *Phys. Rev. Lett.* **38**, 195 (1977).
 - [7] K.-W. Li, T. Hyodo, and L.-S. Geng, *Phys. Rev. C* **98**, 065203 (2018).
 - [8] K. Morita, T. Furumoto, and A. Ohnishi, *Phys. Rev. C* **91**, 024916 (2015).
 - [9] T. Inoue, N. Ishii, S. Aoki, T. Doi, T. Hatsuda, Y. Ikeda, K. Murano, H. Nemura, and K. Sasaki, *Phys. Rev. Lett.* **106**, 162002 (2011).
 - [10] S. R. Beane and et al, *Phys. Rev. Lett.* **106**, 162001 (2011).
 - [11] C. J. Yoon and et al, *Phys. Rev. C* **75**, 022201 (2007).
 - [12] H. Polinder, J. Haidenbauer, and U.-G. Meißner, *Physics Letters B* **653**, 29 (2007).
 - [13] H. Takahashi and et al, *Phys. Rev. Lett.* **87**, 212502 (2001).
 - [14] S. D. Paganis, G. W. Hoffmann, R. L. Ray, J.-L. Tang, T. Udagawa, and R. S. Longacre, *Phys. Rev. C* **62**, 024906 (2000).
 - [15] G. Karl and P. Zenczykowski, *Phys. Rev. D* **36**, 2079 (1987).
 - [16] J. L. Rosner, *Phys. Rev. D* **33**, 2043 (1986).
 - [17] S. A. Yost and C. R. Nappi, *Phys. Rev. D* **32**, 816 (1985).
 - [18] P. B. Mackenzie and H. B. Thacker, *Phys. Rev. Lett.* **55**, 2539 (1985).
 - [19] A. P. Balachandran, A. Barducci, F. Lizzi, V. G. J. Rodgers, and A. Stern, *Phys. Rev. Lett.* **52**, 887 (1984).
 - [20] A. P. Balachandran, A. Barducci, F. Lizzi, V. G. J. Rodgers, and A. Stern, *Phys. Rev. Lett.* **52**, 887 (1984).
 - [21] F. Frömel, B. Juliá-Díaz, and D. Riska, *Nuclear Physics A* **750**, 337 (2005).
 - [22] Y.-R. Liu and M. Oka, *Phys. Rev. D* **85**, 014015 (2012).
 - [23] H. Huang, J. Ping, and F. Wang, *Phys. Rev. C* **87**, 034002 (2013).
 - [24] R. Aaij and et al, *Phys. Rev. Lett.* **119**, 112001 (2017).
 - [25] S.-Q. Luo, K. Chen, X. Liu, Y.-R. Liu, and S.-L. Zhu, *Eur. Phys. J. C* **77**, 709 (2017).
 - [26] T. Mehen, *Phys. Rev. D* **96**, 094028 (2017).
 - [27] C. E. Fontoura, G. Krein, A. Valcarce, and J. Vijande, *Phys. Rev. D* **99**, 094037 (2019).
 - [28] H. Xu, B. Wang, Z.-W. Liu, and X. Liu, *Phys. Rev. D* **99**, 014027 (2019).
 - [29] A. Francis, R. J. Hudspith, R. Lewis, and K. Maltman, *Phys. Rev. D* **99**, 054505 (2019).
 - [30] S. S. Agaev, K. Azizi, and H. Sundu, *Phys. Rev. D* **99**, 114016 (2019).
 - [31] Y. Tan, W. Lu, and J. Ping, *Eur. Phys. J. Plus* **135**, 716 (2020).
 - [32] G. Yang, J. Ping, and J. Segovia, *Phys. Rev. D* **101**, 014001 (2020).
 - [33] J.-B. Cheng, S.-Y. Li, Y.-R. Liu, Z.-G. Si, and T. Yao, *Chin. Phys. C* **45**, 043102 (2021).
 - [34] R. Aaij and et al, *Phys. Rev. D* **102**, 092005 (2020).
 - [35] R. Aaij and et al, *Nat. Phys.* **18**, 751 (2022).
 - [36] T. F. Caramés and A. Valcarce, *Phys. Rev. D* **92**, 034015 (2015).
 - [37] H. Garcilazo and A. Valcarce, *Eur. Phys. J. C* **80**, 720 (2020).
 - [38] H. Huang, J. Ping, and F. Wang, *Phys. Rev. C* **89**, 035201 (2014).
 - [39] Z. Xia, S. Fan, X. Zhu, H. Huang, and J. Ping, *Phys. Rev. C* **105**, 025201 (2022).

- [40] Z. Liu, H.-T. An, Z.-W. Liu, and X. Liu, Doubly charmed dibaryon state (2022), [arXiv:2209.10440 \[hep-ex, physics:hep-ph\]](#)
- [41] X.-W. Wang, Z.-G. Wang, and G.-l. Yu, [Eur. Phys. J. A **57**, 275 \(2021\)](#).
- [42] K. Chen, B.-L. Huang, B. Wang, and S.-L. Zhu, $\sigma_c\sigma_c$ interactions in chiral effective field theory (2022), [arXiv:2204.13316 \[hep-ex, physics:hep-ph\]](#).
- [43] J.-X. Lu, L.-S. Geng, and M. P. Valderrama, [Phys. Rev. D **99**, 074026 \(2019\)](#).
- [44] R. Chen, A. Hosaka, and X. Liu, [Phys. Rev. D **96**, 116012 \(2017\)](#).
- [45] N. Lee, Z.-G. Luo, X.-L. Chen, and S.-L. Zhu, [Phys. Rev. D **84**, 014031 \(2011\)](#).
- [46] N. Li and S.-L. Zhu, [Phys. Rev. D **86**, 014020 \(2012\)](#).
- [47] X.-Z. Ling, M.-Z. Liu, and L.-S. Geng, [Eur. Phys. J. C **81**, 1090 \(2021\)](#).
- [48] W. Meguro, Y.-R. Liu, and M. Oka, [Physics Letters B **704**, 547 \(2011\)](#).
- [49] L. Meng, N. Li, and S.-L. Zhu, [Eur. Phys. J. A **54**, 143 \(2018\)](#).
- [50] Z. Yu, M. Song, J.-Y. Guo, Y. Zhang, and G. Li, [Phys. Rev. C **104**, 035201 \(2021\)](#).
- [51] J. Vijande, A. Valcarce, J.-M. Richard, and P. Sorba, [Phys. Rev. D **94**, 034038 \(2016\)](#).
- [52] Z. Liu, H.-T. An, Z.-W. Liu, and X. Liu, [Phys. Rev. D **105**, 034006 \(2022\)](#).
- [53] X.-K. Dong, F.-K. Guo, and B.-S. Zou, [Commun. Theor. Phys. **73**, 125201 \(2021\)](#).
- [54] S. M. Gerasyuta and E. E. Matskevich, [Int. J. Mod. Phys. E **21**, 1250058 \(2012\)](#).
- [55] Y.-D. Chen and C.-F. Qiao, [Phys. Rev. D **85**, 034034 \(2012\)](#).
- [56] Y.-D. Chen, C.-F. Qiao, P.-N. Shen, and Z.-Q. Zeng, [Phys. Rev. D **88**, 114007 \(2013\)](#).
- [57] H.-X. Chen, D. Zhou, W. Chen, X. Liu, and S.-L. Zhu, [Eur. Phys. J. C **76**, 602 \(2016\)](#).
- [58] C.-F. Qiao, [Physics Letters B **639**, 263 \(2006\)](#).
- [59] C.-F. Qiao, [J. Phys. G: Nucl. Part. Phys. **35**, 075008 \(2008\)](#).
- [60] B.-D. Wan, L. Tang, and C.-F. Qiao, [Eur. Phys. J. C **80**, 121 \(2020\)](#).
- [61] J.-B. Cheng, Z.-Y. Lin, and S.-L. Zhu, [Phys. Rev. D **106**, 016012 \(2022\)](#).
- [62] J. Aguilar and J. M. Combes, [Comm. Math. Phys. **22**, 269 \(1971\)](#).
- [63] E. Balslev and J. M. Combes, [Comm. Math. Phys. **22**, 280 \(1971\)](#).
- [64] P. A. Zyla *et al.* (Particle Data Group Collaboration), [Prog. Theor. Exp. Phys. **2020**, 083C01 \(2020\)](#).
- [65] S. Aoyama, T. Myo, K. Katō, and K. Ikeda, [Prog. Theor. Phys. **116**, 1 \(2006\)](#).
- [66] Y. Ho, [Phys. Rep. **99**, 1 \(1983\)](#).
- [67] E. Hiyaama, Y. Kino, and M. Kamimura, [Prog. Part. Nucl. Phys. **51**, 223 \(2003\)](#).
- [68] T. Noro and H. S. Taylor, [J. Phys. B: At. Mol. Phys. **13**, L377 \(1980\)](#).
- [69] T. N. Rescigno and C. W. McCurdy, [Phys. Rev. A **34**, 1882 \(1986\)](#).
- [70] J. J. Wendoloski and W. P. Reinhardt, [Phys. Rev. A **17**, 195 \(1978\)](#).
- [71] R. M. More and E. Gerjuoy, [Phys. Rev. A **7**, 1288 \(1973\)](#).
- [72] M. Homma, T. Myo, and K. Kato, [Prog. Theor. Phys. **97**, 561 \(1997\)](#).
- [73] H.-Y. Cheng, C.-K. Chua, and A. Soni, [Phys. Rev. D **71**, 014030 \(2005\)](#).
- [74] Y.-R. Liu and M. Oka, [Phys. Rev. D **85**, 014015 \(2012\)](#).